Lowering Synaptogyrin-3 expression rescues Tau-induced memory defects and synaptic loss in the presence of microglial activation

Lowering Synaptogyrin-3 expression rescues Tau-induced memory defects and synaptic loss in the presence of microglial activation

Pablo Largo-Barrientos[1,2], Nuno Apóstolo[1,2], Eline Creemers[1,2], Zsuzsanna Callaerts-Vegh[3], Jef Swerts[1,2], Caitlin Davies[4], Joseph McInnes[1,2], Keimpe Wierda[1,2], Bart De Strooper[1,2,5], Tara Spires-Jones[4], Joris de Wit[1,2], Valerie Uytterhoeven[1,2,#] and Patrik Verstreken[1,2,#,§]

[1] VIB-KU Leuven Center for Brain & Disease Research, Leuven, Belgium

[2] KU Leuven, Department of Neurosciences, Leuven Brain Institute, Mission Lucidity, Leuven, Belgium

[3] KU Leuven, mINT Animal Behavior Facility, Faculty of Psychology, Leuven, Belgium

[4] Centre for Discovery Brain Sciences, University of Edinburgh, Edinburgh, UK

[5] UK Dementia Research Institute, University College London, London, UK

[#] correspondence: valerie.uytterhoeven@kuleuven.vib.be
patrik.verstreken@kuleuven.vib.be

[§] lead contact: patrik.verstreken@kuleuven.vib.be

SUMMARY

Tau is a major driver of neurodegeneration and implicated in over 20 diseases. Tauopathies are characterized by synaptic loss and neuroinflammation, but it is unclear if these pathological events are causally linked. Tau binds to Synaptogyrin-3 on synaptic vesicles. Here, we interfered with this function to determine the role of pathogenic Tau at pre-synaptic terminals. We show that heterozygous knockout of *synaptogyrin-3* is benign in mice, but strongly rescues mutant Tau-induced defects in long-term synaptic plasticity and working memory. It also significantly rescues the pre- and post-synaptic loss caused by mutant Tau. However, Tau-induced neuroinflammation remains clearly upregulated when we remove the expression of one allele of *synaptogyrin-3*. Hence, neuroinflammation is not sufficient to cause synaptic loss and these processes are separately induced in response to mutant Tau. In addition, the pre-synaptic defects caused by mutant Tau are enough to drive defects in cognitive tasks.

INTRODUCTION

Microtubule-associated protein Tau is implicated in numerous neurodegenerative disorders ("tauopathies"), including Alzheimer's disease and traumatic brain injury (Ballatore et al., 2007; Grundke-Iqbal et al., 1986; Wang and Mandelkow, 2016). Tau pathology is observed when the protein causes havoc and aggregates in neurons, and this closely correlates with cognitive decline across these diseases (Arriagada et al., 1992; Duyckaerts et al., 1997). However, the underlying mechanisms that lead to cognitive decline are not fully understood.

When expressed in animal models, mutant human Tau induces cell non-autonomous neuroinflammation, including microglial and astroglial activation (Bellucci et al., 2004; Shi et al., 2017). Similarly, reactive microglia are upregulated in frontotemporal dementia patients carrying a mutation in Tau (Bellucci et al., 2011). These data indicate that pathogenic Tau induces glial activation (Nilson et al., 2017). Expression of Tau in mice also causes the loss of synaptic contacts, and patients suffering from tauopathies display synaptic loss, which correlates well with cognitive decline (Goedert, 2018; Goedert et al., 1991; Iqbal and Novak, 2006; Jackson et al., 2017; Laurent et al., 2018; Leyns and Holtzman, 2017; Tracy and Gan, 2018). Both neuroinflammation and synaptic loss occur simultaneously, ahead of overt aggregation of Tau (Yoshiyama et al., 2007). What is not yet clear is whether activated glial cells and synaptic degeneration are causally linked, and which of these Tau-induced defects are relevant for cognitive decline.

Tau protein is expressed in neurons and under physiological conditions binds to axonal microtubules (Binder et al., 1985). However, mutations and/or hyper-phosphorylation that occur during disease lower the affinity of Tau for microtubules (Dayanandan et al., 1999; Gilley et al., 2016). Detached Tau localizes to dendrites and pre-synaptic terminals (Spires-Jones and Hyman, 2014; Tai et al., 2014) and ectopic Tau at pre-synaptic terminals associates with synaptic vesicles in flies, mice and Alzheimer's disease patients (McInnes et al., 2018; Zhou et al., 2017). Tau-association to synaptic vesicles hampers vesicle mobility, resulting in synaptic dysfunction. Interfering with this binding alleviates Tau-induced vesicle mobility defects in mouse primary neurons *in vitro* and in fruit flies (McInnes et al., 2018; Zhou et al., 2017).

The binding of Tau to vesicles is mediated by Synaptogyrin-3 (Liu et al., 2016; McInnes et al., 2018), a synaptic vesicle-associated protein that belongs to a family of four-pass-transmembrane domain proteins that also includes Synaptogyrin-1, Synaptophysin-1 and Synaptophysin-2/Synaptoporin (Belizaire et al., 2004). Given that Synaptogyrin-3 is uniquely present at pre-synaptic terminals, this allows us to decipher the contribution of pre-synaptic Tau to overall Tau-induced pathology. Here we show that the loss of *synaptogyrin-3* in pathogenic Tau-expressing mice rescues Tau-induced long-term plasticity defects and (pre- and post-) synaptic loss, but not neuroinflammation. Intriguingly, we also find that the loss of *synaptogyrin-3* rescues Tau-induced decline of working memory, and this despite upregulated activated glial cells. Hence, our results indicate that Tau induces neuroinflammation and synaptic loss independently and that synaptic degeneration is a major determinant of cognitive decline.

RESULTS

Synaptogyrin-3 knockout mice are viable and do not show strong phenotypes

We generated a *synaptogyrin-3* knockout mouse line targeting the second exon of the endogenous gene using CRISPR/Cas9 technology (Supplemental figure 1A). *Synaptogyrin-3* knockout mice are viable and fertile and are born in the expected Mendelian inheritance ratios. We validated the efficiency of the knockout with two antibodies that recognize the C- and N-terminal domains of Synaptogyrin-3 protein (Supplemental figure 1B). Synaptogyrin-3 protein is not detected in *synaptogyrin-3*$^{-/-}$ mouse brain homogenates and the expression levels are reduced by half in *synaptogyrin-3*$^{+/-}$ mice (Supplemental figure 1C). The levels of other synaptic proteins including the other neuronally expressed Synaptogyrin, Synaptogyrin-1, are not

significantly different from littermate controls (Supplemental figures 1D-G). Neither *synaptogyrin-3*$^{+/-}$ nor *synaptogyrin-3*$^{-/-}$ mice exhibit obvious visible phenotypes and they are indistinguishable from their wild type littermates in terms of overall appearance (Supplemental figure 1H), body weight (Supplemental figure 1I), motor performance (Supplemental figure 1J) and lifespan (Supplemental figure 1K). Hence, partial or complete loss of Synaptogyrin-3 seem to be well-tolerated in mice over their lifespan.

Synaptogyrin-3 and pathogenic Tau are enriched in mossy fiber-CA3 synapses

We next assessed the immunohistochemical localization of Synaptogyrin-3 in mouse coronal brain sections. We find Synaptogyrin-3 expression across multiple brain regions, including the hippocampus (Figure 1A). The localization pattern that we observe is specific to Synaptogyrin-3 (and does not correspond to Synaptogyrin-1) because we do not detect labeling in *synaptogyrin-3*$^{-/-}$ mice (Figure 1A). Interestingly, when comparing the expression pattern of Synaptogyrin-3 and -1 we detect a strong enrichment of Synaptogyrin-3, compared to Synaptogyrin-1, at the *stratum lucidum* (Figures 1B and 1C). The *stratum lucidum* contains synaptic contacts of dentate gyrus granule cells that send their axons (mossy fibers) to CA3 pyramidal neurons. The mossy fiber-CA3 synapses comprise large pre-synaptic terminals and are critically important for working memory, being altered at early stages of Tau-associated pathology in Alzheimer's Disease patients and mouse models (Viana Da Silva et al., 2019).

Under pathogenic conditions, Synaptogyrin-3 serves as a receptor for Tau at pre-synaptic terminals (McInnes et al., 2018). We therefore assessed where the two proteins localize in mice expressing pathogenic Tau (Tau P301S or 'PS19 mouse line'). We find strong accumulation of Tau in the *stratum lucidum* in six-month-old Tau P301S mice when compared to wild type littermates, while the levels of Tau at other hippocampal layers seem to be similar (Figures 1D and 1E). We observe strong co-labeling of Tau and the pre-synaptic proteins Synaptogyrin-3 and Synaptoporin in the *stratum lucidum* (Figures 1F and 1G), suggesting pre-synaptic accumulation of Tau in mossy fiber-CA3 synapses at this stage.

To verify that pathogenic Tau localizes to Synaptogyrin-3-positive mossy fiber-CA3 synapses we isolated these synapses (Apóstolo et al., 2020) from wild type and Tau P301S mice and labelled them using specific markers. The majority of mossy fiber-CA3 synaptosomes from both wild type and Tau P301S mice are positive for Synaptoporin and Synaptogyrin-3 (Figure 1H), but only the ones from Tau P301S mice are positive for Tau (Figure 1I). A strong co-

localization between Tau and the pre-synaptic proteins Synaptoporin and Synaptogyrin-3 is found in mossy fiber synaptosomes from Tau P301S mice (Figure 1J). Together, these data further confirm that Synaptogyrin-3 and pathogenic Tau are present in the pre-synaptic terminals of mossy fiber-CA3 synapses in six-month-old Tau P301S mice.

Next, we asked if the synaptic-localized Tau associates with vesicles in this model, similar to what we observed in fruit flies and Alzheimer's disease patient brain samples (McInnes et al., 2018; Zhou et al., 2017). We confirm, by western-blotting, that Tau and Synaptogyrin-3 are present in the synaptic vesicle fraction purified from Tau P301S mice, and that there is much less Tau in the synaptic vesicle fraction isolated from wild type littermates (Figure 1K). This difference is not merely because Tau is over-expressed: consistent with previous reports, Tau protein levels are ~5-fold-increased in total Tau P301S mouse brain homogenates compared to wild type mice (Figures 1K and L). However, Tau protein levels are ~13-fold-increased in the synaptic vesicle fraction from Tau P301S mice compared to wild type littermates (Figures 1K and L). Hence, there is significantly more Tau segregating with the synaptic vesicle fraction in Tau P301S mice than the amount of Tau that is over-expressed, consistent with the association of Tau with synaptic vesicles in this model.

Finally, we also tested if Tau and Synaptogyrin-3 co-localize at pre-synaptic terminals in Alzheimer's disease patient brains. We performed array tomography on post-mortem middle/inferior temporal cortical sections (Brodmann area 20/21) from five Braak stage VI Alzheimer's disease patients and five age-matched healthy controls and immunolabeled them using antibodies raised against Synaptogyrin-3, Synapsin-1 (as a general presynaptic marker), and Tau (AF3494 antibody) (Supplemental figure 1L). We find over 33-fold more Synaptogyrin-3-positive puncta that are also positive for Synapsin-1 and Tau in the brain samples from Alzheimer's disease patients compared to healthy control brain samples (2.33% *vs* 0.07%, Supplemental figure 1M). These data indicate that Tau shows increased co-localization with Synaptogyrin-3 at pre-synaptic terminals in the brains of Alzheimer's disease patients compared to healthy controls.

Loss of Synaptogyrin-3 preserves synaptic plasticity in Tau P301S mice

We previously showed that Synaptogyrin-3 mediates pathogenic Tau-induced synaptic dysfunction *in vitro* (McInnes et al., 2018). Here we show that Tau and Synaptogyrin-3 are enriched at mossy fiber-CA3 synapses of Tau P301S mice (Figure 1). We therefore

hypothesized that lowering Synaptogyrin-3 expression in Tau P301S mice would ameliorate pathogenic Tau-induced phenotypes associated with these synapses. We bred Tau P301S mice with *synaptogyrin3*$^{+/-}$ mice and aged the offspring (Supplemental figure 2A). We verified that Synaptogyrin-3 protein expression is ~50% lower in Tau P301S; *synaptogyrin-3*$^{+/-}$ mice compared to Tau P301S littermates (Supplemental figures 2B and C). We also verified that Tau protein expression levels in Tau P301S; *synaptogyrin-3*$^{+/-}$ and Tau P301S littermates are similar (Supplemental figures 2B and C).

We then evaluated the contribution of pathogenic Tau to the synaptic function of mossy fiber-CA3 synapses by assessing the electrophysiological properties of these synapses in acute hippocampal slices of 6-7-month-old Tau P301S mice (Figure 2A). We verified that the recordings belong to mossy fiber-CA3 synapses by application of DCG-IV (Figure 2A), a group II metabotropic glutamate receptors (mGluR) agonist that selectively depresses mossy fiber transmission (Nicoll and Schmitz, 2005). When we apply incremental single stimulations to mossy fibers we find that the post-synaptic potentials at the *stratum lucidum* of Tau P301S and wild type littermate controls are indistinguishable (Supplemental figure 2D), indicating general excitability is not affected. Next, we applied paired-pulse stimulations and find the ratios of the amplitudes of the responses in Tau P301S mice and wild type controls to be similar (Supplemental figure 2E). This indicates that pathogenic Tau does not affect short-term plasticity of mossy fiber-CA3 synapses at early stages of pathology. Hence, pathogenic Tau does not affect the basic synaptic transmission characteristics of mossy fiber-CA3 synapses.

Next, we measured long-term plasticity and applied a three-theta-burst-stimulation (TBS) paradigm to the mossy fibers to induce long-term potentiation (LTP). When compared to wild type controls, we find that expression of pathogenic Tau limits the induction and maintenance of LTP (Figure 2B). Given that LTP is mostly determined by pre-synaptic components in mossy fiber-CA3 synapses (Nicoll and Schmitz, 2005), we hypothesize that reduction of Synaptogyrin-3 levels can ameliorate this Tau-induced LTP-defect. We recorded LTP of mossy fiber-CA3 synapses in 6-7-month-old Tau P301S; *synaptogyrin-3*$^{+/-}$ mice and find a response similar to that of their wild type littermates and higher than that of Tau P301S mice (Figures 2B-E). Reduction of Synaptogyrin-3 in wild type animals does not have an effect on the LTP response, as LTP recordings from *synaptogyrin-3*$^{+/-}$ mice are comparable to those from wild type littermates (Figures 2B-E). Thus, reduction of Synaptogyrin-3 levels corrects long-term plasticity defects induced by pathogenic Tau at mossy fiber-CA3 synapses.

We also tested if lowering Synaptogyrin-3 expression affects Tau-induced defects at other synapses and recorded LTP of Schaffer collateral-CA1 synapses (Supplemental figure 2F). Whereas LTP of mossy fiber-CA3 synapses originates from pre-synaptic mechanisms, LTP of Schaffer collateral-CA1 synapses is induced by post-synaptic NMDAR signalling and expressed by increased AMPAR activity (Lledo et al., 1998; Lüscher et al., 1999). When we record LTP of Schaffer collateral-CA1 synapses on 6-7-month-old mice we find no differences between wild type and Tau P301S (Supplemental figure 2G). This is likely explained because at this age, the accumulation of Tau in Tau P301S mice is mostly restricted to the CA3 *stratum lucidum* (Figure 1D). However, when we record LTP in eight-month-old Tau P301S mice, an age at which Tau accumulation is already extended towards the CA1 hippocampal region, we find that LTP of Schaffer collateral-CA1 synapses is severely impaired. Interestingly, removing the expression of one copy of *synaptogyrin-3* (Tau P301S; *synaptogyrin-3*$^{+/-}$) rescues this defect (Supplemental figures 2H-K). These findings suggest that the positive effect of reducing Synaptogyrin-3 levels is not restricted to synapses with a strong pre-synaptic component like mossy fiber-CA3 synapses but that the same applies to other synapses, like Schaffer collateral-CA1 synapses.

Loss of Synaptogyrin-3 reverts working memory defects in Tau P301S mice

Long-term synaptic plasticity underlies mechanisms of learning and memory. We therefore assessed learning and memory capacity of Tau P301S and wild type mice in two different versions of the Morris Water Maze (MWM) test, reflecting separate aspects of cognition. A classic MWM protocol where the platform location does not change assesses *spatial reference memory* that is largely under control of CA1 pyramidal neurons or "place cells" (Morris et al., 1982). An alternative MWM paradigm evaluates *working memory*, for which CA3 pyramidal neurons are essential (Nakazawa et al., 2003). In this paradigm the location of the platform remains constant for only a single day but changes between days, thus representing a higher cognitive challenge for the mice (see STAR Methods for details).

In mice that are 6-7 months old, a stage at which Schaffer collateral-CA1 LTP is not yet affected (Supplemental figure 2G), we do not find a significant difference in the *spatial reference memory* test between Tau P301S mice and littermate controls (Supplemental figures 3A-C). However, in the *working memory* test, 6-7-month-old Tau P301S mice perform worse than their wild type littermates: they fail to significantly reduce the path length needed to find the platform over consecutive swims (Supplemental figure 3D). These results are in line with impaired LTP

of mossy fiber-CA3 synapses at this stage in Tau P301S mice (Figure 2). We verified that the defect in *working memory* is not influenced by sex (Supplemental figure 3E). We also verified that the *working memory* defect in Tau P301S mice is not of developmental origin as 3-4-month-old Tau P301S mice do improve their performance over consecutive swims (Supplemental figure 3F). Given that reduction of Synaptogyrin-3 corrects pathogenic Tau-induced defects in LTP of mossy fiber-CA3 synapses, we next asked whether this also corrects the *working memory* defect in 6-7-month-old Tau P301S mice. Tau P301S; *synaptogyrin-3*$^{+/-}$ mice perform as well as wild type mice and they are more efficient than Tau P301S mice in adapting to the novel spatial locations, as evidenced by statistically significant reduction of path lengths and time (latency) needed to find the platform (Figure 3). Hence, working memory defects are directly induced by pre-synaptic pathogenic Tau and are dependent on the presence of the pre-synaptic protein Synaptogyrin-3.

Lowering Synaptogyrin-3 levels prevents synaptic loss in Tau P301S mice

A common feature in patients suffering from tauopathies and in mice expressing pathogenic Tau is the loss of synapses, especially in the hippocampus (Spires-Jones and Hyman, 2014). We evaluated the total area occupied by mossy fiber-CA3 synapses in Tau P301S mice using immunohistochemistry. We labelled mossy fiber-CA3 synapses of 8-9-month-old mice with two different pre- and post-synaptic *stratum lucidum* markers, Synaptoporin and Synapsin-3 (both pre-synaptic markers) as well as GluK5 and Nectin-3 (both enriched post-synaptically), and find all these markers to be reduced in Tau P301S mice compared to wild type littermates (Figure 4A and supplemental figure 4A). We then tested if lowering Synaptogyrin-3 levels is sufficient to prevent this defect. We find that the synaptic *stratum lucidum* area labelled by these markers in Tau P301S; *synaptogyrin-3*$^{+/-}$ mice is similar to wild type littermates (Figure 4B and supplemental figure 4B). Consistently, in western blots of hippocampal homogenates we also observe that the protein levels of Synapsin-3 and GluK5 are lower in Tau P301S mice but similar to wild type controls in Tau P301S; *synaptogyrin-3*$^{+/-}$ mice (supplemental figures 4C and D). This rescue of synaptic integrity is not because Tau expression is altered in Tau P301S; *synaptogyrin-3*$^{+/-}$ mice, because the *stratum lucidum* area in these animals is labelled by Tau (Supplemental figure 4E). Together, these data indicate that the synaptic loss induced by mutant Tau is rescued by lowering Synaptogyrin-3 expression.

To further corroborate our observations, we also performed transmission electron microscopy visualizing mossy fiber-CA3 synapses in wild type, *synaptogyrin-3*$^{+/-}$, Tau P301S and Tau

P301S; *synaptogyrin-3*$^{+/-}$ mice (Figure 4C). Mossy fiber-CA3 synapses are easily identified by their large pre-synaptic boutons and because they have a high density of synaptic vesicles. We quantified the number of mossy fiber boutons in standard-sized images and find their number is reduced in Tau P301S mice. In contrast, Tau P301S; *synaptogyrin-3*$^{+/-}$ show a number of mossy fiber boutons per area similar to wild type or *synaptogyrin-3*$^{+/-}$ mice (Figure 4D). We find the average area of the remaining individual mossy fiber boutons to be smaller in Tau P301S mice, but in Tau P301S; *synaptogyrin-3*$^{+/-}$ mice their size is comparable to wild type littermates (Figure 4E). We also measured the number of synaptic release sites normalized to bouton perimeter (Supplemental figure 4F). We find less release sites in Tau P301S mice compared to wild type littermates and we observe this defect is rescued in Tau P301S; *synaptogyrin-3*$^{+/-}$ mice (Supplemental figure 4G). Thus, we conclude that lowering Synaptogyrin-3 levels in animals that express pathogenic Tau preserves synaptic integrity.

Tau-induced activation of astrocytes and microglia does not depend on Synaptogyrin-3

Expression of pathogenic Tau in mice induces cell non-autonomous activation of microglia and astroglia (Yoshiyama et al., 2007). Tau-activated glial cells are thought to engulf and degrade synaptic contacts (Vogels et al., 2019). However, it is unclear how pathogenic Tau triggers glial activation and whether this activation is indeed essential for synaptic loss. We labeled mouse coronal brain sections with the microglial marker Iba1 and with the astrocytic marker GFAP. We find that 8-9-month-old Tau P301S mice show an important increase in the total number of astrocytes and microglia in the *stratum lucidum* (Figures 4F-I). Interestingly, compared to littermate controls, Tau P301S; *synaptogyrin-3*$^{+/-}$ mice show a similar increase in astrocytes and microglia (Figures 4F-I); this is despite the rescue of synaptic degeneration in these animals (Figures 4A-E). We analysed the morphology of the GFAP-positive and Iba1-positive cells and find that the majority of them in both P301S and Tau P301S; *synaptogyrin-3*$^{+/-}$ mice contain abundant thick processes, typical of reactive astrocytes and activated microglia (Figures 4F and H). The cellular state of activated microglia is characterized by a set of damage-activated microglia (DAM) genes. We measured DAM gene expression in the hippocampus using quantitative RT-PCR. This further confirms the increased level of microglial activation in mice expressing Tau P301S but also, to the same extent, in Tau P301S; *synaptogyrin-3*$^{+/-}$ animals (Figure 4J). Expression of microglial homeostatic genes is also increased (although less than DAM genes) in Tau P301S and in Tau P301S; *synaptogyrin-3*$^{+/-}$ mice (Supplemental Figure 4H). These data indicate that Tau-induced synaptic degeneration and neuroinflammation can

be uncoupled and that synapses can be preserved in the presence of a surrounding neuroinflammatory response.

DISCUSSION

Mutant Tau causes multifactorial defects including pre- and post-synaptic loss and neuroinflammation (Liu et al., 2004; Rapoport et al., 2002; Roberson et al., 2007). It has however been difficult to genetically separate these functions and assess their pathophysiological relevance. In this work we interfered with the pre-synaptic-specific function of pathogenic Tau by lowering the levels of Synaptogyrin-3, a synaptic vesicle-associated protein. We find that lowering *synaptogyrin-3* expression protects neurons that express pathogenic Tau from synaptic plasticity defects, synaptic loss and decline in working memory, indicating that pre-synaptic tau pathology mediates all these defects. We find this rescue, despite the presence of activated glial cells, suggesting that Tau induces neuroinflammation and synaptic defects independently.

Synaptic dysfunction is one of the earliest events associated with Tau-induced pathology (Clare et al., 2010). Mutant or hyperphosphorylated Tau dissociates from microtubules causing the protein to excessively localize to synaptic terminals. Tau P301S mice express pathogenic Tau protein pan-neuronally, but Tau accumulation is initially enriched at the *stratum lucidum*, which contains mossy fiber-CA3 synapses. This allows us to assess specific aspects of pre-synaptic Tau-induced pathology by focusing on these synapses, which are also enriched in Synaptogyrin-3. Previous studies found that Tau and Synaptogyrin-3 interact (Liu et al., 2016; McInnes et al., 2018) causing the clustering of synaptic vesicles (McInnes et al., 2018; Zhou et al., 2017). Our data now indicate that Synaptogyrin-3 is critical to unchain a series of harmful events that eventually lead to cognitive impairment and synaptic loss, two common features seen in tauopathies.

Tau also relocates to somato-dendritic areas and enters the post-synaptic region to contribute to synaptic dysfunction (Hoover et al., 2010; Ittner et al., 2010). We show that correcting insults induced by Tau at pre-synaptic terminals is sufficient to restore synaptic function- and memory-defects. Our work first tested the synaptic plasticity of mossy fiber-CA3 synapses, which is compromised upon expression of pathogenic Tau and rescued upon reduction of *synapogyrin-3* expression. However, the “rescuing effect” we observe appears to be a general feature across synapses, including Schaffer collateral-CA1 synapses where LTP is encoded post-synaptically.

This indicates that preventing Tau-induced presynaptic pathology has a beneficial effect at post synaptic terminals. It will be interesting to assess if targeting the presynaptic defects induced by Tau have consequences for the trans-synaptic spreading of the protein, and whether this is a mechanism by which lowering of a presynaptic protein induces rescue of Tau-induced defects in post-synaptic processes.

The presence of pathogenic Tau causes a neuroinflammatory response (Laurent et al., 2018). We show that Tau-induced synapse degeneration and cognitive impairment can be rescued even in the presence of glial activation. This implies that Tau-associated neuroinflammatory responses do not directly depend on synaptic dysfunction. Activated microglia and astroglia are associated with early stages of Tau-induced pathology in Alzheimer patient brains and mouse models (Leyns and Holtzman, 2017; Yoshiyama et al., 2007). Neurons accumulating pathogenic Tau expose factors that recruit and activate glial cells by acting on microglial and astrocytic receptors (Lastres-Becker et al., 2014; Sidoryk-Węgrzynowicz and Strużyńska, 2019), but it seems they do so independently of the synaptic dysfunction. However, the precise mechanisms through which Tau induces the expression or secretion of those factors remain unknown.

Several studies have suggested that activated microglia can engulf and degrade synapses that accumulate Tau (Laurent et al., 2018; Dejanovic et al., 2018). However, it is not clear whether Tau-induced microglial activation is *necessary* and/or *sufficient* to induce synaptic loss. Our results now add an important element and indicate that activated microglia alone are not *sufficient* to lower the presynaptic content. By manipulating the expression of a protein that is specifically expressed within pre-synaptic terminals, we show that Tau-induced degeneration of synapses can be prevented despite Tau-induced neuroinflammation. This suggests a model in which the interaction of pathogenic Tau and Synaptogyrin-3 at pre-synapses is *necessary* to cause synaptic loss, without excluding that activated microglia also subsequently play a role. Further research will now be needed to determine whether these observations translate to other tauopathy mouse models and to complex tauopathies like Alzheimer's disease, where amyloid-β pathology also induces a neuroinflammatory response (Zhong et al., 2018).

Finally, our work suggests that Synaptogyrin-3 is a promising target to tackle tauopathies. Synaptogyrin-3 is exclusively expressed in neurons and resides on synaptic vesicles (Belizaire et al., 2004). We show that heterozygous (and also homozygous) knockout of Synaptogyrin-3 is -at the level of our analyses- benign in mice. Mice and humans express two neuronal

Synaptogyrins, Synaptogyrin-1 and -3, and together with Synaptophysin-1 and -2 they constitute a major family of evolutionary conserved tyrosine-phosphorylated four-transmembrane domain proteins (Takamori et al., 2006). Previous studies reported phenotypes only when several of the four "gyrin- and physin- proteins" were depleted simultaneously. Loss of *synaptogyrin-1* and *synaptophysin-1* caused defects in synaptic plasticity of Schaffer collateral-CA1 synapses (Janz et al., 1999), whereas deletion of all four proteins led to elevated synaptic vesicle release probability at Calyx of Held synapses and Schaffer collateral-CA1 synapses (Raja et al., 2019). Our study shows that *synaptogyrin-3*$^{-/-}$ mice are viable, fertile and their lifespan is comparable to that of their wild type littermates. Furthermore, our analyses indicate that *synaptogyrin-3*$^{+/-}$ mice do not exhibit defects in synaptic function at mossy fiber-CA3 synapses nor at Schaffer collateral-CA1 synapses. This suggests redundant functions of neuronal Synaptogyrins and Synaptophysins (Janz et al., 1999; Raja et al., 2019) and together the data suggest that reducing the levels of Synaptogyrin-3 to tackle tauopathies is relatively safe.

Our work provides evidence that it is possible to rescue synapse degeneration and memory impairment in a tauopathy mouse model by targeting pre-synaptic Tau. Reducing the levels of Synaptogyrin-3 is sufficient to prevent dysfunction and elimination of synapses accumulating pathogenic Tau, even though proliferation and activation of microglia and astroglia are still present. This work thus shows that synaptic degeneration and neuroinflammation are separately induced responses to Tau pathology. Future work will be essential to determine the therapeutic potential of interfering with Synaptogyrin-3 and pre-synaptic Tau.

ACKNOWLEDGEMENTS

We thank the VIB-KU Leuven Center for Brain & Disease Research mouse expertise unit, electrophysiology expertise unit, light microscopy expertise unit and electron microscopy expertise unit for help. We thank members of the Verstreken lab for input and discussion. Research support was provided by two ERC consolidator grants (P.V and T.S-J.), an ERC starting grant (J.d.W.) and an FWO Odysseus grant (J.d.W), the Research Foundation Flanders (FWO), the Hercules Foundation, a Methusalem grant of the Flemish government, the Alzheimer Association and Tau consortium, IMI2, Opening the Future (Leuven University fund), Alzheimer Research Foundation (SAO-FRA), the UK Dementia Research Institute (which receives funding from the UK Medical Research Council, Alzheimer's Society and Alzheimer's Research UK) and VIB. P.L.-B is supported by a fellowship from the FWO, N.A.

by a fellowship from the Fundação para a Ciência e a Tecnologia (FCT) and J.M. by a fellowship from the BAEF. P.V. and T.S.-J. are alumni of the FENS Kavli Network of Excellence.

AUTHOR CONTRIBUTIONS

P.L.-B. and P.V. conceived the study, designed experiments, analysed data and wrote the manuscript. E.C. performed electrophysiology, J.S. performed electron microscopy, Z.C.-V. performed behaviour experiments and C.D. performed the array tomography. P.L-B. performed the other experiments. K.W. helped to design, perform and analyse electrophysiology experiments. N.A., J.M. T.S.-J. and V.U. helped in the overall design of the study and provided assistance with experiments. B.D.S. and J.d.W. provided critical feedback. All authors read and approved the final version of the manuscript.

DECLARATION OF INTERESTS

The authors declare no competing interests.

STAR METHODS

LEAD CONTACT AND MATERIALS AVAILABILITY

Further information and requests for resources and reagents should be directed to and will be fulfilled by the Lead Contact, Patrik Verstreken (patrik.verstreken@kuleuven.vib.be).

EXPERIMENTAL MODEL AND SUBJECT DETAILS

General observations

All mice experiments were conducted according to the KU Leuven ethical guidelines and approved by the KU Leuven Ethical Committee for Animal Experimentation. Mice were maintained in a specific pathogen-free (SPF) facility under standard housing conditions, on a diurnal 12-hour light/dark cycle and with continuous access to food and water. Male mice were used for electrophysiology experiments and female mice were used for behavior experiments. In both cases, small cohorts of males and females were tested in pilot experiments and sex differences were not found. Both males and females were indistinctly used for immunostainings, transmission electron microscopy experiments and synaptosome isolation.

Generation of *synaptogyrin-3* knockout mice

The *synaptogyrin-3* knockout mice were generated in the VIB-KU Leuven Center for Brain & Disease Research Mouse Expertise Unit using CRISPR/Cas9 technology. The forward guide RNA targeting the second exon of mouse *SYNGR3* gene was selected using CRISPOR tool (sequence: 5'-TTCGGACCGATTGTCAACGA-3'). The single-stranded oligo DNA insertion cassette consisted of three stop codons disturbing the three different open reading frames and one EcoRI restriction site (to simplify the genotyping protocol) flanked by two homology arms (sequence: 5'-GTGAGGCTCTGCTTGCTGCTCTGCAGGTGTTTTCTATTGCGGTGTTCGGACCGATTGTCAATAACTAGATGAGAATTCCGAGGGCTACGTGAACTCCGACAGTGGTCCAGAACTGCGCTGCGTCTTCAACGGAAATGC-3'). The CRISPR/Cas9 system efficiency was tested by transfection of the ribonucleoprotein (RNP) complex (purified Cas9, guide RNA and single-stranded oligo DNA, all from Integrated DNA Technologies, IDT) into mouse embryonic fibroblasts with lipofectamine RNAiMAX (Thermo Fisher Scientific). Genomic DNA was extracted 48 hours after transfection and homologous recombination at the cleaving

site was checked by PCR with insertion-specific designed primers (forward primer sequence: 5'-GTCAATAACTAGATGAGAATTCCGAG-3' and reverse primer sequence: 5'-CTGAGAAGCCCAGGTCCAG-3'). Next, C57BL/6 zygotes were injected with the RNP complex and transferred to CD1 foster females and the offspring was screened for integration of the intended sequence in the mouse *SYNGR3* locus. Genomic DNA was extracted from mice ear-punches using KAPA Mouse Genotyping HotStart Kit (KAPA Biosystems) and PCR was performed with the previously described insertion-specific primers. Insertion was confirmed by Sanger sequencing. Mice that were positive for insertion were back-crossed with C57BL/6 mice for three generations to remove possible off-site insertions and since then, the colony was maintained by mating *synaptogyrin-3*$^{-/-}$ animals. Genotypes were checked by DNA extraction from ear-punches and PCR amplification of a mouse *SYNGR3* gene region flanking the insertion site (forward primer sequence: 5'-GAAC-TCTGGGGCAGGTATGG-3' and reverse primer sequence: 5'-TACATTAGGCCCCGCCT-TTC-3'). PCR products were digested with EcoRI restriction enzyme and samples were loaded onto a QIAxcel DNA screening cartridge (QIAGEN). Those samples that gave a single DNA band of 367 bp were assigned to wild type mice, those that gave two DNA bands of 241 and 137 bp were assigned to *synaptogyrin-3*$^{-/-}$ mice and those that gave three DNA bands of 367, 241 and 137 bp were assigned to *synaptogyrin-3*$^{+/-}$ mice.

Breeding of Tau P310S and *synaptogyrin-3* knockout mice

The Tau P301S mouse model (or PS19) was previously generated (Yoshiyama et al., 2007) and was obtained from Jackson laboratories (B6;C3-Tg(Prnp-MAPT*P301S)PS19Vle/J, stock number 008169). The colony was maintained by mating hemizygous Tau P301S and C57BL/6 mice. Genotypes were checked by DNA extraction from ear-punches and PCR using human Tau P301S transgene-specific primers (forward primer sequence: 5'-GGGGACACGTCTCCACGGCATCTCAGCAATGT-CTCC-3' and reverse primer sequence: 5'-TCCCCCAGCCTAGACCACGAGAAT-3'). Tau P301S mice were mated with *synaptogyrin-3*$^{+/-}$ mice and genotypes of the offspring were determined as previously described for Tau P301S mice and *synaptogyrin-3* knockout mice.

Human subjects

Use of human tissue for post-mortem studies was approved by the Edinburgh Brain Bank ethics committee and the medical research ethics committee (the Academic and Clinical

Central Office for Research and Development, a joint office of the University of Edinburgh and NHS Lothian, approval number 15-HV-016). The Edinburgh Brain Bank is a Medical Research Council funded facility with research ethics committee (REC) approval (11/ES/0022). Demographic details for participants in this study can be found in Supplemental Table 1.

METHOD DETAILS

Immunostaining of mouse coronal brain sections

Mice were anesthetized with isoflurane and decapitated. Brains were dissected, embedded in tissue optimal cutting temperature (OCT) compound (QPath medium, VWR) and frozen in dry ice-cold isopentane. Coronal 18 µm-thick sections were cut using a cryostat (NX70, Thermo Fisher Scientific) and collected onto SuperFrost Ultra Plus adhesion slides (Thermo Fisher Scientific). Sections were fixed in 1:1 acetone:methanol for 5 minutes at -20 ºC and washed in PBS. In some cases, heat-induced antigen retrieval was performed by heating the sections in 0.1 M sodium citrate (pH 6) up to boiling for three times. Sections were permeabilized in PBS containing 0.05% Triton X-100 for 20 minutes at room temperature and blocked in PBS containing 0.5% Triton X-100 and 5% normal goat serum (blocking solution) for 2 hours at room temperature. In the case of immunostaining with primary antibodies produced in mice, anti-mouse IgG antigen-binding fragments (Jackson ImmunoResearch) were added 1:50 to the blocking solution. Subsequently, sections were incubated with primary antibodies in blocking solution overnight at 4 ºC, washed in PBS and incubated with secondary antibodies in blocking solution for 2 hours at room temperature. Finally, sections were washed in PBS, incubated with 0.1 µg/mL DAPI in PBS for 5 minutes at room temperature and washed again in PBS, and coverslips were mounted on top of the sections with Mowiol (Sigma-Aldrich). Imaging was performed at the VIB-KU Leuven Center for Brain and Disease Research Light Microscopy Expertise Unit. Overview images of the hippocampus were acquired with a Nikon spinning-disk microscope with a 10X/0.5 N.A. lens. Images of the CA3 region were acquired with a Nikon A1R confocal microscope with a 20X/1.0 N.A. lens or a 60X/1.0 N.A. lens. Images were analyzed and processed using Fiji software (National Institutes of Health).

Isolation and immunostaining of mouse mossy fiber-CA3 synaptosomes

Mice were anesthetized with isoflurane and decapitated. Brains were extracted and hippocampi were dissected in ice-cold Hanks Balanced Salt Solution. Hippocampi from five wild type or Tau P301S mice were pulled together and homogenized in homogenization buffer (0.32 M sucrose, 4 mM HEPES and 1 mM $MgCl_2$) at pH 7.4 and supplemented with protease inhibitors (pepstatin A, leupeptin, aprotinin and PMSF). Homogenized hippocampi solutions were filtered subsequently through 100 µm, 70 µm and 30 µm cell strainers (Miltenyi Biotec) and filtered samples were centrifuged for 20 minutes at 1,000 x g and 4 ºC. The pellets containing mossy fiber-CA3 synaptosomes were resuspended in homogenization buffer and centrifuged as in the previous step. Washed pellets were resuspended in PBS and incubated with myelin-removing magnetic beads (Miltenyi Biotec) for 20 minutes at 4 ºC with rotation. Samples were centrifuged for 10 minutes at 1,000 x g and 4 ºC to remove the beads-containing buffer and pellets were resuspended in PBS and passed through PBS-washed columns mounted on a magnet to remove the beads. Myelin-depleted samples were transferred to PDL-coated 8-well chamber slides (Thermo Fisher Scientific) and incubated for 90 minutes at 4 ºC while shaking to let synaptosomes settle. Synaptosome preparations were fixed in PBS containing 2% paraformaldehyde and 2% glucose for 15 minutes at room temperature, washed in PBS and permeabilized and blocked in PBS containing 3% bovine serum albumin and 0.1% saponin (blocking solution) for 30 minutes at room temperature. Subsequently, synapstosome preparations were incubated with primary antibodies in blocking solution overnight at 4 ºC, washed in PBS and incubated with secondary antibodies in blocking solution for 2 hours at room temperature. Finally, synaptosome preparations were washed in PBS, incubated with 0.1 µg/mL DAPI in PBS for 5 minutes at room temperature and washed again in PBS, and coverslips were mounted with Mowiol (Sigma-Aldrich). Images of mossy fiber-CA3 synaptosomes were acquired with a Nikon A1R confocal microscope with a 60X/1.0 N.A. lens. Images were analyzed and processed using Fiji software (National Institutes of Health).

Isolation of synaptic vesicle fraction from mouse brain

Mice were anesthetized with isoflurane and decapitated. Brains were extracted and homogenized in homogenization buffer (0.32 M sucrose, 4 mM HEPES and 1 mM $MgCl_2$) at pH 7.4 and supplemented with protease inhibitors (Complete Protease Inhibitor Cocktail, Roche). Homogenized brain solutions were centrifuged for 10 min at 1,000 x g and 4 ºC and supernatants were further centrifuged for 15 min at 10,000 x g and 4 ºC. Pellets containing synatosomes were resuspended in homogenization buffer and centrifuged as in the previous

step. Washed pellets were resuspended in a hypotonic buffer (5 mM HEPES at pH 7.4 supplemented with Complete Protease Inhibitor Cocktail) and incubated for 30 min at 4 ºC with rotation. After osmotic shock, samples containing lysed synaptosomes were centrifuged for 20 min at 25,000 x g and 4 ºC to remove mitochondria and membrane debris and supernatants were further centrifuged for 2 h at 165,000 x g and 4 ºC (both using a Beckmann Optima TL-100 ultracentrifuge). The resulting pellets containing synaptic vesicles were resuspended in buffer containing 5 mM HEPES and 0.3 M glycine at 7.4 and lysed in RIPA Lysis and Extraction Buffer (Thermo Fisher Scientist) for protein quantification by western blotting.

Array tomography of human brain tissue

Cortical tissue samples from Brodmann area (BA) 20/21 of Alzheimer's disease and age-matched control patients were collected at autopsy, dissected into small cortical blocks and fixed in 20 mM PBS containing 4% paraformaldehyde and 2.5% sucrose for 2 h. Samples were then dehydrated in ascending grades of cold ethanol, embedded in LR white resin and polymerised at 56°C for 24 h. Embedded tissue was sectioned into 70 nm-thick serial sections and tissue ribbons were collected on gelatin coated coverslips. For immunolabeling, tissue ribbons were incubated in 50 mM glycine for 5 min and subjected to antigen retrieval in citrate buffer (10 mM citric acid and 0.05% Tween 20 at pH 6.0) using a pressure cooker. Ribbons were blocked in TBS containing 0.05% Tween 20 and 0.1% fish skin gelatin for 30 min, incubated overnight with primary antibodies in blocking solution, washed in TBS and incubated for 30 min with secondary antibodies in blocking solution. Finally, ribbons were incubated with 10 µg/mL DAPI and coverslips were mounted with Immu-Mount (Thermo Fisher Scientist). Images were acquired at the same location in each serial section using a Zeiss AxioImager Z2 epifluorescent microscope with a 63x/1.4 N.A. Plan Apochromat objective equipped with a CoolSnap digital camera. Serial sequences of images were converted into stacks and aligned using ImageJ and MATLAB. Custom MATLAB scripts were then used to threshold image stacks and determine density and co-localization of markers. Markers were considered to co-localize when at least 25% of their area overlapped with the other marker/s of interest.

Electrophysiological field recordings on acute mouse hippocampal slices

Electrophysiology was performed at the VIB-KU Leuven Center for Brain and Disease Research Electrophysiology Expertise Unit. Mice were anesthetized with isoflurane and decapitated. Brains were dissected and transferred into ice-cold cutting solution (87 mM NaCl, 2.5 mM KCl, 1.25 mM NaH_2PO_4, 10 mM glucose, 25 mM $NaHCO_3$, 0.5 mM $CaCl_2$, 7 mM $MgCl_2$, 75 mM sucrose, 1 mM kynurenic acid, 5 mM ascorbic acid and 3 mM pyruvic acid) at pH 7.4 and 5% CO_2/ 95% O_2. Parasagittal hippocampal 300 µm-thick sections were cut using a vibratome (VT1200 Leica) and incubated at 34ºC for 35 min to recover. For recordings, slices were placed onto a multielectrode array (MEA 2100, Multichannel Systems) and continuously perfused with room-temperature artificial cerebrospinal fluid (aCSF) solution (125 mM NaCl, 2.5 mM KCl, 1.25 mM NaH_2PO_4, 25 mM glucose, 25 mM $NaHCO_3$, 1 mM $MgSO_4 \cdot 7H_2O$ and 2 mM $CaCl_2$) at pH 7.4 and 5% CO_2/ 95% O_2. Field excitatory post-synaptic potentials (fEPSPs) were recorded from mossy fiber-CA3 synapses or Schaffer collateral-CA1 synapses by stimulating and recording from the appropriate electrodes. First, input-output curves were established for each individual slice by applying single-stimuli ranging from 500 to 2,750 mV with 250 mV increments. Stimulus strength that corresponds to 35% of maximal response in the input-output curve was applied for the following recordings. Paired-pulse facilitation experiments were performed by applying paired stimuli with 25, 50, 100, 200 and 400 ms inter-stimulus intervals. For long-term potentiation (LTP) experiments, stable fEPSPs were recorded for 30 minutes to establish a baseline. Afterwards, three trains of high-frequency stimulation (100 stimuli at 100 Hz) with 5 min intervals were applied to induce LTP and fEPSPs were recorded for 65 additional minutes. fEPSPs were recorded every 3 min in response to three consecutive stimulations (15 s apart), and the amplitude of each three consecutive fEPSPs was averaged. Recordings were analyzed and processed using Multi Channel Experimenter software (Multichannel Systems).

Morris water maze tests

Mice were transferred to the mINT Animal Behavior Facility at the KU Leuven Faculty of Psychology two weeks before the behavioral experiments for habituation. Two different protocols based on the Morris water maze test were used. For both protocols, mice were trained in four daily swims to locate a hidden 15 cm-diameter platform in a 150 cm-diameter circular pool filled with tempered (26 ± 1 ºC), opacified water (Acusol Opacifier, Dow Chemicals). For each protocol, experimentally naïve animals were used. During the *spatial reference memory* protocol, the location of the platform remained fixed over the entire training period of ten days and the starting swim positions were randomly chosen from four

defined locations (starting positions 1, 3, 5 and 7 in Figure 3A). On days 6 and 11, the platform was removed and probe trials (100 seconds) were performed to assess spatial reference memory. During the *working memory* protocol, the position of the hidden platform changed every day (platform locations shown in Figure 3A) and starting swim positions were located in the opposite semicircle. Prior to *working memory* testing, mice were trained for three days with a flagged visible platform used in all four swims on day 1, in the first two sims on day 2 and only in the first swim on day 3. This adaptation trained the animal to daily changes of platform location and forced the animal to use distal cues for spatial orientation. Swim paths were recorded by an overhead camera and parameters such as path length, swim speed, latency to reach the platform, floating behavior and average distance to the platform were extracted from the track files using Ethovision software (Noldus).

RNA isolation, cDNA synthesis and real-time quantitative PCR (RT-qPCR)

Mice were anesthetized with isoflurane and decapitated. Brains were extracted and hippocampi were dissected in ice-cold PBS. RNA extraction was carried out with mirVana PARIS kit (Thermo Fisher Scientific), according to the instructions provided by the manufacturer. cDNA synthesis from RNA samples was performed with SuperScript II One-Step RT-CR System with Platinum Taq DNA Polymerase (Thermo Fisher Scientific). For each cDNA sample, 25 ng were loaded onto a 384-wells plate and SensiFAST SYBR No-ROX mix and primers were added. RT-qPCR was performed in a LightCycler 480 instrument (Roche).

Protein extraction and western blotting

Mice were anesthetized with isoflurane and decapitated. Brains were dissected and homogenized in RIPA Lysis and Extraction Buffer (Thermo Fisher Scientific) with a Dounce homogenizer. Samples were lysed for 30 minutes at 4 ºC with rotation and lysates were centrifuged for 15 minutes at 4 ºC and 14,000 rpm to pellet debris. Protein concentration was measured in cleared lysates using Bradford Assay (Bio-Rad) and samples were boiled in Laemmli Sample Buffer (Bio-Rad) for 5 minutes at 95 ºC. Equal amounts of protein samples were loaded in NuPAGE Novex 4-12% Bis-Tris gels (Invitrogen Novex) for protein separation by electrophoresis performed in MOPS SDS Running Buffer (Invitrogen Novex). Proteins were transferred to nitrocellulose membranes (Bio-Rad) with Trans-Blot Turbo Transfer system (Bio-Rad). Membranes were washed in TBS containing 0.1% Tween 20

(TBS-T) and blocked in TBS-T with 5% milk powder (blocking solution). Membranes were subsequently incubated with primary antibodies in blocking solution overnight at 4 ºC, washed in TBS-T, incubated with secondary antibodies in blocking solution for one hour at room temperature and washed again in TBS-T. Membranes were incubated with Western Lightning Plus-ECL (Perkin Elmer) and protein bands were visualized and imaged by chemiluminescence in a LAS-3000 Mini instrument (Fujifilm). Images were analyzed and processed using Fiji software (National Institutes of Health).

Transmission electron microscopy

Mice were anesthetized by intraperitoneal administration of 1 µL/g xylazine (XYL-M 2%, VetCompendium), 2 µL/g ketamine (100 mg/mL, Eurovet Nimatek) and 3 µL/g salne (0.9%). Mice were subjected to transcardial perfusion with fixative solution (4% paraformaldehyde, 2.5% glutaraldehyde and 0.2% picric acid in 0.1M Phosphate Buffer) and brains were dissected and post-fixed in fixative solution overnight at 4ºC. Subsequently, brains were washed in 0.1M Phosphate Buffer, embedded in 3% agarose (Sigma-Aldrich) and 80 µm-thick coronal sections were cut using a vibratome (VT1000S, Leica). Hippocampal CA3 regions were cropped from the brain sections and cropped sections were post-fixed in 0.1M Phosphate Buffer containing 1% OsO_4 and 1.5% $K_4Fe(CN)_6$ for one hour at room-temperature and incubated in 25% methanol with 0.5% uranyl acetate overnight at 4 ºC with rotation. After, sections were washed in ddH_2O and incubated with Walton's lead aspartate (0.02 M lead nitrate in 0.03 M sodium aspartate, pH 5.5) for 30 minutes at 60 ºC, washed again in ddH_2O and dehydrated with graded series of ethanol (30%, 50%, 70%, 80%, 95% and 100%). Finally, sections were infiltrated with propylene oxide:resin (2:1, 1:1 and 1:2 supplemented with BDMA) and embedded in pure EPON resin. Ultrathin 70 nm-thick sections were cut using an ultramicrotome (EM UC7, Leica) and collected on copper grids. Images of mossy fiber-CA3 synapses were acquired with a JEOL JEM1400 transmission electron microscope equipped with an Olympus SIS Quemesa camera with 2500X or 5000X magnification. Images were analyzed and processed using Fiji software (National Institutes of Health).

QUANTIFICATION AND STATISTICAL ANALYSIS

Quantification was performed using Fiji (National Institutes of Health), Multi Channel Experimenter (Multichannel Systems) and Ethovision (Noldus) software, depending on the experiment. All graphs depict mean ± SEM. For statistical analyses, datasets were tested for

normality using D'Agostino and Pearson test. When datasets passed normality test they were analyzed using Student's t-test or one- or two-way ANOVA with Tukey's or Dunnett's multiple comparisons tests. In all cases, *p*-values and *N* numbers are shown in the graphs. The *N* values correspond to the number of animals used for a specific experiment, unless otherwise specified.

DATA AND CODE AVAILABILITY

NA.

REFERENCES

Apóstolo, N., Smukowski, S.N., Vanderlinden, J., Condomitti, G., Rybakin, V., ten Bos, J., Trobiani, L., Portegies, S., Vennekens, K.M., Gounko, N. V., et al. (2020). Synapse type-specific proteomic dissection identifies IgSF8 as a hippocampal CA3 microcircuit organizer. Nat. Commun. *11*.

Arriagada, P. V., Growdon, J.H., Hedley-Whyte, E.T., and Hyman, B.T. (1992). Neurofibrillary tangles but not senile plaques parallel duration and severity of Alzheimer's disease. Neurology *42*, 631–639.

Ballatore, C., Lee, V.M.Y., and Trojanowski, J.Q. (2007). Tau-mediated neurodegeneration in Alzheimer's disease and related disorders. Nat. Rev. Neurosci. *8*, 663–672.

Belizaire, R., Komanduri, C., Wooten, K., Chen, M., Thaller, C., and Janz, R. (2004). Characterization of synaptogyrin 3 as a new synaptic vesicle protein. J. Comp. Neurol. *470*, 266–281.

Bellucci, A., Westwood, A.J., Ingram, E., Casamenti, F., Goedert, M., and Spillantini, M.G. (2004). Induction of inflammatory mediators and microglial activation in mice transgenic for mutant human P301S tau protein. Am. J. Pathol. *165*, 1643–1652.

Bellucci, A., Bugiani, O., Ghetti, B., and Spillantini, M.G. (2011). Presence of reactive microglia and neuroinflammatory mediators in a case of frontotemporal dementia with P301S mutation. Neurodegener. Dis. *8*, 221–229.

Binder, L.I., Frankfurter, A., and Rebhun, L.I. (1985). The distribution of tau in the mammalian central nervous system. J. Cell Biol. *101*, 1371–1378.

Clare, R., King, V.G., Wirenfeldt, M., and Vinters, H. V. (2010). Synapse loss in dementias. J. Neurosci. Res. *88*, 2083–2090.

Dayanandan, R., Van Slegtenhorst, M., Mack, T.G., Ko, L., Yen, S.H., Leroy, K., Brion, J.P., Anderton, B.H., Hutton, M., and Lovestone, S. (1999). Mutations in tau reduce its microtubule binding properties in intact cells and affect its phosphorylation. FEBS Lett. *446*, 228–232.

Dejanovic, B., Huntley, M.A., De Mazière, A., Meilandt, W.J., Wu, T., Srinivasan, K., Jiang,

Z., Gandham, V., Friedman, B.A., Ngu, H., et al. (2018). Changes in the Synaptic Proteome in Tauopathy and Rescue of Tau-Induced Synapse Loss by C1q Antibodies. Neuron *100*, 1322-1336.e7.

Duyckaerts, C., Uchihara, T., Seilhean, D., He, Y., and Hauw, J.J. (1997). Dissociation of Alzheimer type pathology in a disconnected piece of cortex. Acta Neuropathol. *93*, 501–507.

Gilley, J., Ando, K., Seereeram, A., Rodríguez-Martín, T., Pooler, A.M., Sturdee, L., Anderton, B.H., Brion, J.-P., Hanger, D.P., and Coleman, M.P. (2016). Mislocalization of neuronal tau in the absence of tangle pathology in phosphomutant tau knockin mice. Neurobiol. Aging *39*, 1–18.

Goedert, M. (2018). Tau filaments in neurodegenerative diseases. FEBS Lett. *592*, 2383–2391.

Goedert, M., Spillantini, M.G., and Crowther, R.A. (1991). Tau proteins and neurofibrillary degeneration. Brain Pathol. *1*, 279–286.

Grundke-Iqbal, I., Iqbal, K., Quinlan, M., Tung, Y.C., Zaidi, M.S., and Wisniewski, H.M. (1986). Microtubule-associated protein tau. A component of Alzheimer paired helical filaments. J. Biol. Chem. *261*, 6084–6089.

Hoover, B.R., Reed, M.N., Su, J., Penrod, R.D., Kotilinek, L.A., Grant, M.K., Pitstick, R., Carlson, G.A., Lanier, L.M., Yuan, L.-L., et al. (2010). Tau Mislocalization to Dendritic Spines Mediates Synaptic Dysfunction Independently of Neurodegeneration. Neuron *68*, 1067–1081.

Iqbal, K., and Novak, M. (2006). From tangles to tau protein. Bratisl. Lek. Listy *107*, 341–342.

Ittner, L.M., Ke, Y.D., Delerue, F., Bi, M., Gladbach, A., van Eersel, J., Wölfing, H., Chieng, B.C., Christie, M.J., Napier, I.A., et al. (2010). Dendritic Function of Tau Mediates Amyloid-β Toxicity in Alzheimer's Disease Mouse Models. Cell *142*, 387–397.

Jackson, J.S., Witton, J., Johnson, J.D., Ahmed, Z., Ward, M., Randall, A.D., Hutton, M.L., Isaac, J.T., O'Neill, M.J., and Ashby, M.C. (2017). Altered Synapse Stability in the Early Stages of Tauopathy. Cell Rep. *18*, 3063–3068.

Janz, R., Südhof, T.C., Hammer, R.E., Unni, V., Siegelbaum, S.A., and Bolshakov, V.Y. (1999). Essential roles in synaptic plasticity for synaptogyrin I and synaptophysin I. Neuron *24*, 687–700.

Lastres-Becker, I., Innamorato, N.G., Jaworski, T., Rábano, A., Kügler, S., Van Leuven, F., and Cuadrado, A. (2014). Fractalkine activates NRF2/NFE2L2 and heme oxygenase 1 to restrain tauopathy-induced microgliosis. Brain *137*, 78–91.

Laurent, C., Buée, L., and Blum, D. (2018). Tau and neuroinflammation: What impact for Alzheimer's Disease and Tauopathies? Biomed. J. *41*, 21–33.

Leyns, C.E.G., and Holtzman, D.M. (2017). Glial contributions to neurodegeneration in tauopathies. Mol. Neurodegener. *12*.

Liu, C., Song, X., Nisbet, R., and Götz, J. (2016). Co-immunoprecipitation with Tau isoform-specific antibodies reveals distinct protein interactions and highlights a putative role for 2N Tau in disease. J. Biol. Chem. *291*, 8173–8188.

Liu, T., Perry, G., Chan, H.W., Verdile, G., Martins, R.N., Smith, M.A., and Atwood, C.S. (2004). Amyloid-β-induced toxicity of primary neurons is dependent upon differentiation-associated increases in tau and cyclin-dependent kinase 5 expression. J. Neurochem. *88*, 554–563.

Lledo, P.M., Zhang, X., Südhof, T.C., Malenka, R.C., and Nicoll, R.A. (1998). Postsynaptic membrane fusion and long-term potentiation. Science *279*, 399–403.

Lüscher, C., Xia, H., Beattie, E.C., Carroll, R.C., von Zastrow, M., Malenka, R.C., and Nicoll, R.A. (1999). Role of AMPA receptor cycling in synaptic transmission and plasticity. Neuron *24*, 649–658.

McInnes, J., Wierda, K., Snellinx, A., Bounti, L., Wang, Y.-C., Stancu, I.-C., Apóstolo, N., Gevaert, K., Dewachter, I., Spires-Jones, T.L., et al. (2018). Synaptogyrin-3 Mediates Presynaptic Dysfunction Induced by Tau. Neuron *97*, 823-835.e8.

Morris, R.G.M., Garrud, P., Rawlins, J.N.P., and O'Keefe, J. (1982). Place navigation impaired in rats with hippocampal lesions. Nature *297*, 681–683.

Nakazawa, K., Sun, L.D., Quirk, M.C., Rondi-Reig, L., Wilson, M.A., and Tonegawa, S.

(2003). Hippocampal CA3 NMDA receptors are crucial for memory acquisition of one-time experience. Neuron *38*, 305–315.

Nicoll, R.A., and Schmitz, D. (2005). Synaptic plasticity at hippocampal mossy fibre synapses. Nat. Rev. Neurosci. *6*, 863–876.

Nilson, A.N., English, K.C., Gerson, J.E., Barton Whittle, T., Nicolas Crain, C., Xue, J., Sengupta, U., Castillo-Carranza, D.L., Zhang, W., Gupta, P., et al. (2017). Tau oligomers associate with inflammation in the brain and retina of tauopathy mice and in neurodegenerative diseases. J. Alzheimer's Dis. *55*, 1083–1099.

Raja, M.K., Preobraschenski, J., Olmo-Cabrera, S. Del, Martinez-Turrillas, R., Jahn, R., Perez-Otano, I., and Wesseling, J.F. (2019). Elevated synaptic vesicle release probability in synaptophysin/gyrin family quadruple knockouts. Elife *8*.

Rapoport, M., Dawson, H.N., Binder, L.I., Vitek, M.P., and Ferreira, A. (2002). Tau is essential to beta -amyloid-induced neurotoxicity. Proc. Natl. Acad. Sci. U. S. A. *99*, 6364–6369.

Roberson, E.D., Scearce-Levie, K., Palop, J.J., Yan, F., Cheng, I.H., Wu, T., Gerstein, H., Yu, G.-Q., and Mucke, L. (2007). Reducing Endogenous Tau Ameliorates Amyloid -Induced Deficits in an Alzheimer's Disease Mouse Model. Science (80-.). *316*, 750–754.

Shi, Y., Yamada, K., Liddelow, S.A., Smith, S.T., Zhao, L., Luo, W., Tsai, R.M., Spina, S., Grinberg, L.T., Rojas, J.C., et al. (2017). ApoE4 markedly exacerbates tau-mediated neurodegeneration in a mouse model of tauopathy. Nature *549*, 523–527.

Sidoryk-Węgrzynowicz, M., and Strużyńska, L. (2019). Astroglial contribution to tau-dependent neurodegeneration. Biochem. J. *476*, 3493–3504.

Spires-Jones, T.L., and Hyman, B.T. (2014). The Intersection of Amyloid Beta and Tau at Synapses in Alzheimer's Disease. Neuron *82*, 756–771.

Tai, H.C., Wang, B.Y., Serrano-Pozo, A., Frosch, M.P., Spires-Jones, T.L., and Hyman, B.T. (2014). Frequent and symmetric deposition of misfolded tau oligomers within presynaptic and postsynaptic terminals in Alzheimer's disease. Acta Neuropathol. Commun. *2*.

Takamori, S., Holt, M., Stenius, K., Lemke, E.A., Grønborg, M., Riedel, D., Urlaub, H.,

Schenck, S., Brügger, B., Ringler, P., et al. (2006). Molecular anatomy of a trafficking organelle. Cell *127*, 831–846.

Tracy, T.E., and Gan, L. (2018). Tau-mediated synaptic and neuronal dysfunction in neurodegenerative disease. Curr. Opin. Neurobiol. *51*, 134–138.

Viana Da Silva, S., Zhang, P., Haberl, M.G., Labrousse, V., Grosjean, N., Blanchet, C., Frick, A., and Mulle, C. (2019). Hippocampal mossy fibers synapses in CA3 pyramidal cells are altered at an early stage in a mouse model of Alzheimer's disease. J. Neurosci. *39*, 4193–4205.

Vogels, T., Murgoci, A.-N., and Hromádka, T. (2019). Intersection of pathological tau and microglia at the synapse. Acta Neuropathol. Commun. *7*.

Wang, Y., and Mandelkow, E. (2016). Tau in physiology and pathology. Nat. Rev. Neurosci. *17*, 5–21.

Yoshiyama, Y., Higuchi, M., Zhang, B., Huang, S.-M., Iwata, N., Saido, T.C., Maeda, J., Suhara, T., Trojanowski, J.Q., and Lee, V.M.-Y. (2007). Synapse Loss and Microglial Activation Precede Tangles in a P301S Tauopathy Mouse Model. Neuron *53*, 337–351.

Zhong, L., Wang, Z., Wang, D., Wang, Z., Martens, Y.A., Wu, L., Xu, Y., Wang, K., Li, J., Huang, R., et al. (2018). Amyloid-beta modulates microglial responses by binding to the triggering receptor expressed on myeloid cells 2 (TREM2). Mol. Neurodegener. *13*, 15.

Zhou, L., McInnes, J., Wierda, K., Holt, M., Herrmann, A.G., Jackson, R.J., Wang, Y.-C., Swerts, J., Beyens, J., Miskiewicz, K., et al. (2017). Tau association with synaptic vesicles causes presynaptic dysfunction. Nat. Commun. *8*, 15295.

Figure 1. Synaptogyrin-3 and pathogenic Tau are enriched in mossy fiber-CA3 synapses.

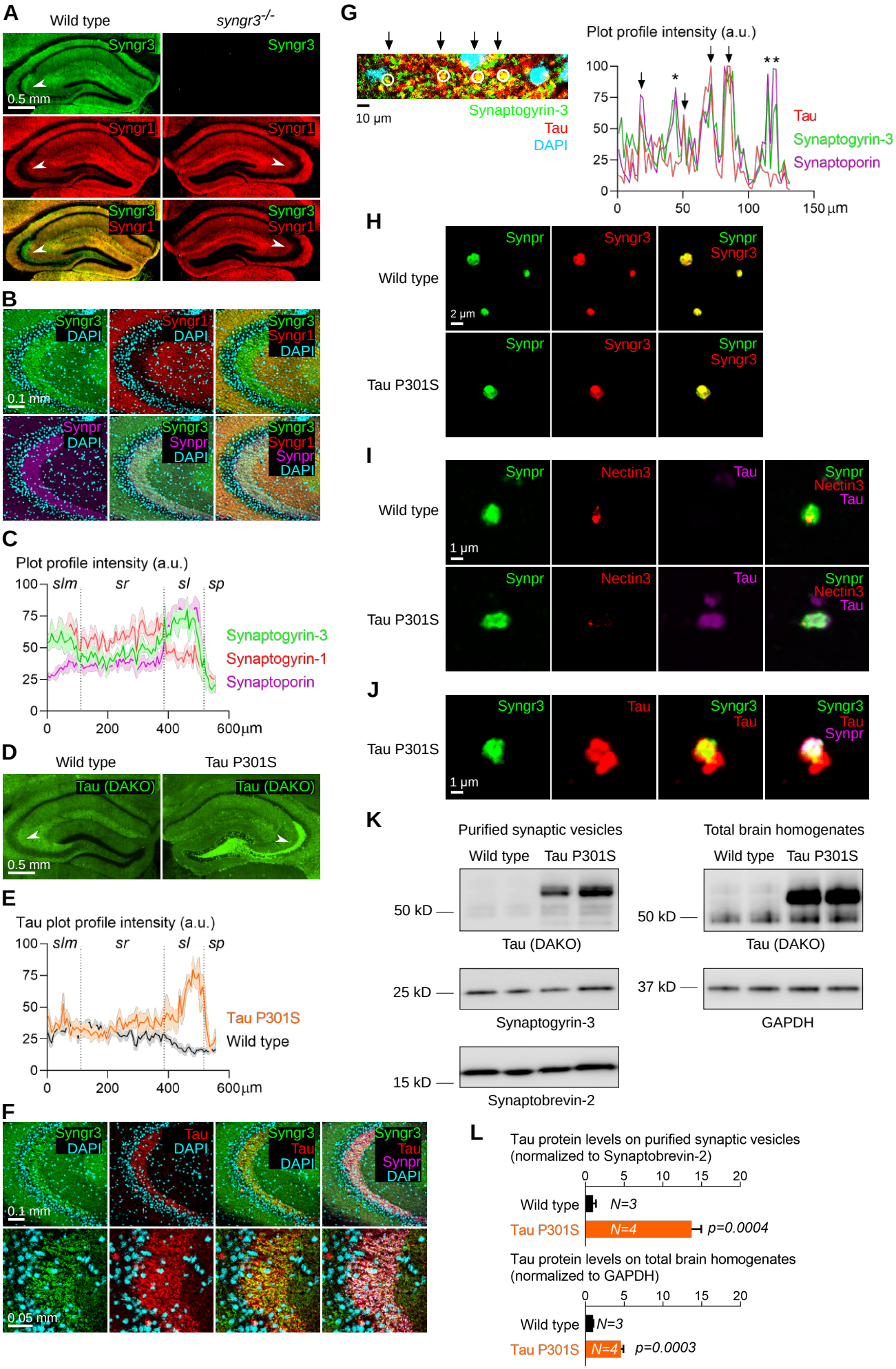

Figure 2. Loss of Synaptogyrin-3 in a tauopathy mouse model corrects defects in synaptic long-term plasticity.

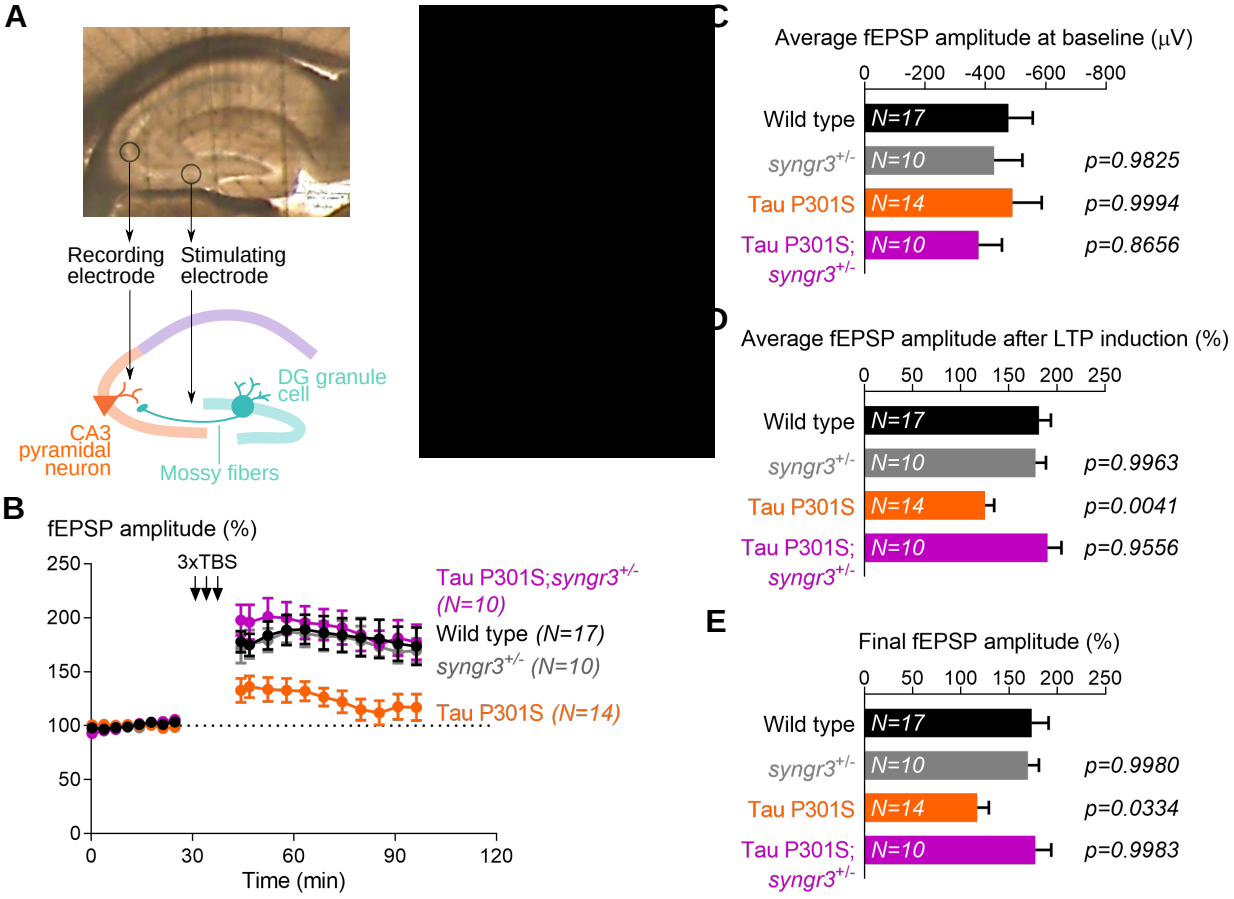

Figure 3. Loss of Synaptogyrin-3 in a tauopathy mouse model corrects cognitive impairment.

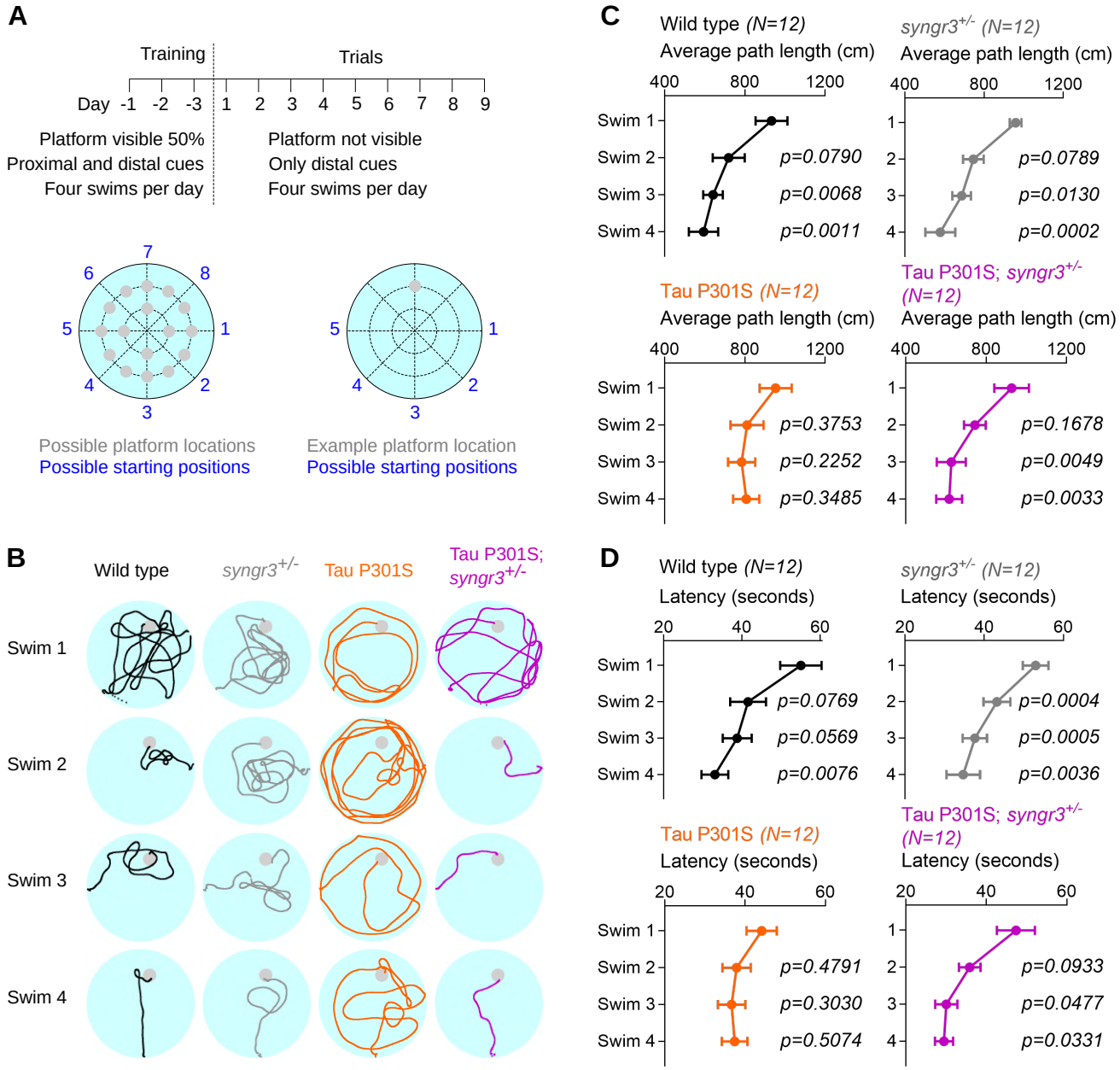

Figure 4. Loss of Synaptogyrin-3 in a tauopathy mouse model prevents synaptic loss independently of glial proliferation and activation.

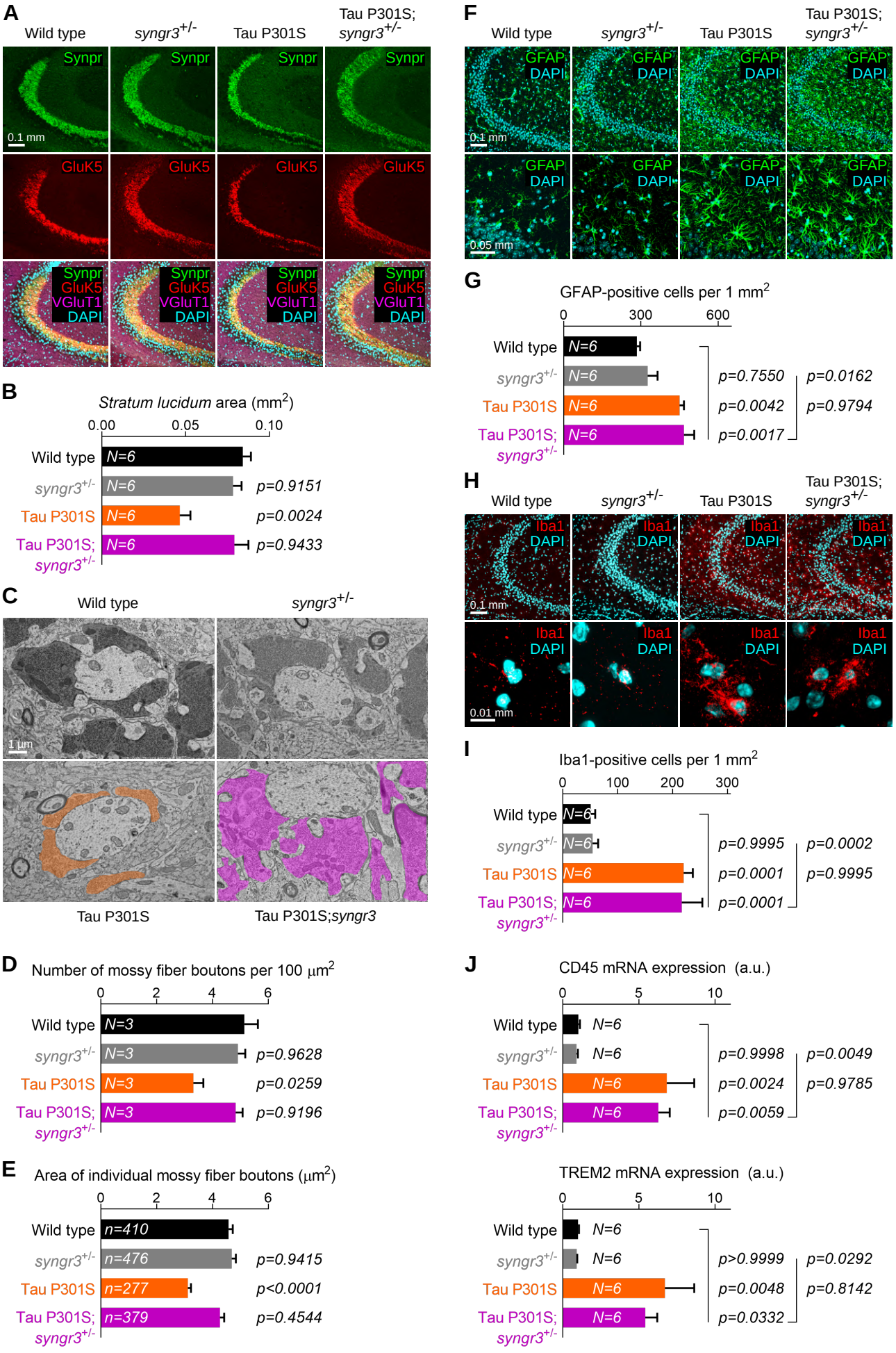

FIGURE LEGENDS

Figure 1. Synaptogyrin-3 and pathogenic Tau are enriched in mossy fiber-CA3 synapses.
(A) Coronal hippocampal sections from six-month-old wild type and *synpatogyrin-3*$^{-/-}$ mice immunolabeled for Synaptogyrin-3 and Synaptogyrin-1. Arrowheads point to *stratum lucidum.*
(B) Confocal images of the wild type mouse hippocampal CA3 region immunolabeled for Synaptogyrin-3, Synaptogyrin-1, Synaptophysin-2/Synaptoporin and DAPI.
(C) Plot profile of the intensity for Synaptogyrin-3, Synaptogyrin-1 and Synaptophysin-2/Synaptoporin across the CA3 hippocampal layers *stratum lacnosum-moleculare* (slm), *stratum radiatum* (sr), *stratum lucidum* (sl) and *stratum pyramidale* (sp). Graph depicts the average intensity (± SEM) of each synaptic marker (as percentage of maximal intensity) calculated from six separate images.
(D) Coronal hippocampal sections from six-month-old wild type and Tau P301S mice immunolabeled for Tau (DAKO antibody).
(E) Plot profile of the intensity for Tau across the CA3 hippocampal layers *stratum lacnosum-moleculare* (slm), *stratum radiatum* (sr), *stratum lucidum* (sl) and *stratum pyramidale* (sp). Graph depicts the average intensity (± SEM) of Tau (as percentage of maximal intensity) calculated from five separate images.
(F) Confocal images of the Tau P301S mouse hippocampal CA3 region immunolabeled for Synaptogyrin-3, Tau (DAKO antibody), Synaptophysin-2/Synaptoporin and DAPI.
(G) Left, high magnification confocal image within the Tau P301S mouse hippocampal CA3 region immunolabeled for Synaptogyrin-3, Tau (DAKO antibody) and DAPI. Arrows point to spots where Synaptogyrin-3 and Tau overlap (circled). Right, plot profile of the intensity (as percentage of maximal intensity) for Tau, Synaptogyrin-3 and Synaptophysin-2/Synaptoporin across the image shown on the left. Arrows mark peaks of high intensity for Tau, Synaptogyrin-3 and Synaptophysin-2/Synaptoporin (representing synaptic spots positive for Tau) and stars mark peaks of high intensity for Synaptogyrin-3 and Synaptophysin-2/Synaptoporin and not for Tau (representing synaptic spots negative for Tau).
(H) Confocal images of mossy fiber-CA3 synaptosomes isolated from six-month-old wild type and Tau P301S mice and immunolabeled for Synaptogyrin-3 and Synaptophysin-2/Synaptoporin.
(I) Confocal images of mossy fiber-CA3 synaptosomes isolated from six-month-old wild type and Tau P301S mice and immunolabeled for Synaptophysin-2/Synaptoporin, Nectin-3 and Tau (DAKO antibody).

(J) Confocal images of mossy fiber-CA3 synaptosomes isolated from six-month-old wild Tau P301S mice and immunolabeled for Synaptogyrin-3, Tau (DAKO antibody) and Synaptophysin-2/Synaptoporin.

(K) Immunoblotting of purified synaptic vesicle fractions and brain homogenates from six-month-old wild type and Tau P301S mice for Tau (DAKO antibody), Synaptogyrin-3, Synaptobrevin-2 and GAPDH.

(K) Quantification of Tau protein levels on purified synaptic vesicle fractions (normalized to Synaptobevin-2 protein levels) and brain homogenates (normalized to GAPDH protein levels) from six-month-old wild type and Tau P301S mice. Graphs depict mean ± SEM and statistical significance was calculated using Student's unpaired t-test.

Figure 2. Lowering Synaptogyrin-3 expression preserves synaptic plasticity in Tau P301S mice.

(A) Top, image of a mouse acute hippocampal slice on the multielectrode array (MEA2100, Multichannel Systems) used for field excitatory post-synaptic potential (fEPSP) recordings. Bottom, schematic diagram indicating stimulation of mossy fibers and recording at CA3 *stratum lucidum.* Right, an example fEPSP recording from mossy fiber-CA3 synapses showing a dramatic reduction of fEPSP amplitude upon application of group II metabotropic glutamate receptors (mGluR) agonist DCG-IV, and the full recovery upon washing with artificial cerebrospinal fluid (aCSF).

(B) fEPSPs were recorded from mossy fiber-CA3 synapses in 6-7-month-old wild type, *synaptogyrin-3*$^{+/-}$, Tau P301S and Tau P301S; *synaptogyrin-3*$^{+/-}$ mice. After 30 min of stable baseline recordings, long-term potentiation (LTP) was induced by applying three trains of high-frequency (100 Hz) stimulation and fEPSPs were recorded for 75 additional min. Graph depicts mean ± SEM of the amplitude from each three consecutive recordings (15 s apart), represented as percentage of baseline average.

(C) Average amplitude of the fEPSPs recorded before LTP induction (baseline). Graph depicts mean ± SEM and statistical significance was calculated using one-way ANOVA with Tukey's multiple comparisons test (*p*-values compared to wild type mice).

(D) Average amplitude of the fEPSPs recorded after LTP induction and represented as percentage of the average amplitude of the fEPSPs recorded at baseline. Graph depicts mean ± SEM and statistical significance was calculated using one-way ANOVA with Tukey's multiple comparisons test (*p*-values compared to wild type mice).

(E) Amplitude of the last three fEPSPs recorded 65 min after LTP induction and represented as percentage of the average amplitude of the fEPSPs recorded at baseline. Graph depicts mean ± SEM and statistical significance was calculated using one-way ANOVA with Tukey's multiple comparisons test (*p*-values compared to wild type mice).

Figure 3. Lowering Synaptogyrin-3 expression reverts working memory defects in Tau P301S mice.

(A) Experimental design based on the working memory protocol in the Morris water maze by Nakazawa et al., 2003 (see STAR Methods).

(B) Representative swim tracks of six-seven-month-old wild type, *synaptogyrin-3*$^{+/-}$, Tau P301S and Tau P301S; *synaptogyrin-3*$^{+/-}$ mice over four daily swims.

(C) Average path length (distance swam to find the platform) per swim (1-4) and genotype. Graphs depict mean ± SEM and statistical significance was calculated using two-way ANOVA with Tukey's multiple comparisons test (*p*-values compared to swim 1).

(D) Average latency (time needed to find platform) per swim (1-4) and genotype. Graphs depict mean ± SEM and statistical significance was calculated using two-way ANOVA with Tukey's multiple comparisons test (*p*-values compared to swim 1).

Figure 4. Reduction of Synaptogyrin-3 in Tau P301S mice prevents synaptic loss independent of glial proliferation and activation.

(A) Confocal images of the hippocampal CA3 region of eight-nine-month-old wild type, *synaptogyrin-3*$^{+/-}$, Tau P301S and Tau P301S; *synaptogyrin-3*$^{+/-}$ mice immunolabeled for Synaptophysin-2/Synaptoporin, Glutamate Kainate receptor 5 (GluK5), Vesicular Glutamate Transporter 1 (VGluT1) and DAPI.

(B) Quantification of the total area occupied by the *stratum lucidum* (Synaptoporin and GluK5 double-positive region). Graph depicts mean ± SEM and statistical significance was calculated using one-way ANOVA with Tukey's multiple comparisons test (*p*-values compared to wild type mice).

(C) Electron micrographs of mossy fiber-CA3 synapses from eight-nine-month-old wild type, *synaptogyrin-3*$^{+/-}$, Tau P301S and Tau P301S; *synaptogyrin-3*$^{+/-}$ mice. Mossy fiber boutons are highlighted in color.

(D) Quantification of the number of mossy fiber boutons in a 100 µm^2-area. Graph depicts mean ± SEM and statistical significance was calculated using one-way ANOVA with Tukey's multiple comparisons test (*p*-values compared to wild type mice).

(E) Quantification of the average area of individual mossy fiber boutons. Graph depicts mean ± SEM and statistical significance was calculated using one-way ANOVA with Tukey's multiple comparisons test (*p*-values compared to wild type mice). The *n* values correspond to the number of boutons analyzed from at least three animals per genotype.

(F) Confocal images of the hippocampal CA3 region of 8-9-month-old wild type, *synaptogyrin-3*$^{+/-}$, Tau P301S and Tau P301S; *synaptogyrin-3*$^{+/-}$ mice immunolabeled for astrocytic marker GFAP and DAPI.

(G) Quantification of the number of GFAP-positive cells in a 1 mm^2-area. Graph depicts mean ± SEM and statistical significance was calculated using one-way ANOVA with Tukey's multiple comparisons test (*p*-values on the left compared to wild type mice and *p*-values on the right compared to Tau P301S; *synaptogyrin-3*$^{+/-}$ mice).

(H) Confocal images of the hippocampal CA3 region of 8-9-month-old wild type, *synaptogyrin-3*$^{+/-}$, Tau P301S and Tau P301S; *synaptogyrin-3*$^{+/-}$ mice immunolabeled for microglial marker Iba1 and DAPI.

(I) Quantification of the number of Iba1-positive cells in a 1 mm^2-area. Graph depicts mean ± SEM and statistical significance was calculated using one-way ANOVA with Tukey's multiple comparisons test (*p*-values on the left compared to wild type mice and *p*-values on the right compared to Tau P301S; *synaptogyrin-3*$^{+/-}$ mice).

(J) Expression of disease associated microglial (DAM) response genes CD45 and TREM2 in hippocampal homogenates from eight-nine-month-old wild type, *synaptogyrin-3*$^{+/-}$, Tau P301S and Tau P301S; *synaptogyrin-3*$^{+/-}$ mice. Expression levels were analyzed by quantitative RT-PCR and normalized to Actin and GAPDH expression in wild type mice. Graph depicts mean ± SEM and statistical significance was calculated using one-way ANOVA with Tukey's multiple comparisons test (*p*-values on the left compared to wild type mice and *p*-values on the right compared to Tau P301S; *synaptogyrin-3*$^{+/-}$ mice).